Journal of Thermal Science Vol.32, No.3 (2023) 1007−1022

https://doi.org/10.1007/s11630-023-1794-y **Article ID: 1003-2169(2023)03-1007-16**

Relationship between the Intensity of Secondary Flow and Convection Heat Transfer in a Helically Coiled Circular Tube with Uniform Wall Temperature

ZHANG Jinlong[1,2], ZHAO Chuangyao[3], WANG Liangbi[1,2*]

1. School of Mechanical Engineering, Lanzhou Jiaotong University, Lanzhou, Gansu 730070, China
2. Key Laboratory of Railway Vehicle Thermal Engineering of MOE, Lanzhou Jiaotong University, Lanzhou 730070, China
3. School of Building Services Science and Engineering, Xi'an University of Architecture and Technology, Xi'an 710055, China

Abstract: Numerical method is used to investigate fully developed laminar flow in helically coiled circular tube in this paper. The non-dimensional parameter (secondary flow Reynolds number *Se*) based on absolute vorticity flux along the mainstream is used to indicate the intensity of secondary flow caused by the centrifugal effect in helically coiled circular tube. The relationship between the intensity of secondary flow and the intensity of laminar convective heat transfer is studied. The effects of curvature and torsion on the enhancement of heat transfer are also considered. The results reveal that the absolute vorticity flux along the mainstream can be used to indicate the local or averaged intensity of secondary flow; the non-dimensional parameter of the absolute vortex along the main flow determines the convective heat transfer and friction factor. The relationships of Nusselt number and friction factor with the *Se* are obtained. The effect of curvature on Nusselt number is obvious, but the effect of torsion on Nusselt number is less obvious.

Keywords: helically coiled circular tube, convective heat transfer, heat transfer enhancement, secondary flow

1. Introduction

Secondary flow is a flow perpendicular to the mainstream direction. Due to the existence of secondary flow, the flow becomes very complex. Secondary flow enhances the mixing of fluid and enhances heat transfer. In helically coiled circular tube, under the action of centrifugal force, there is a laminar flow even at a larger Reynolds number, and secondary flow appears [1]. The dimensionless number commonly used to describe coils and elbows is Dean number, and its most common form is $Dn=Re(d/D)^{0.5}$ [2, 3]. It includes the Reynolds number *Re* and the structural parameters of tube. Many scholars also use the above *Dn* number to describe the flow in helically coiled circular tube. However, helically coiled circular tube is more complex than the coil pipe. The inlet and outlet of the coil pipe are in the same plane, and the central axis of the inlet and outlet of a helically coiled circular tube differs by a pitch.

Recent years, flow in helically coiled tubes has frequently been considered numerically and experimentally. The study of Liberto et al. show that affected by secondary flow the heat transfer on outer side surface of curved tube is strengthened, while the heat

Article Type: Contributed by the 8th Asian Symposium on Computational Heat Transfer and Fluid Flow (ASCHT-2021)
GE: TANG Guihua
Received: Feb 26, 2022 Corresponding author: WANG Liangbi E-mail: lbwang@mail.lzjtu.cn

List of symbols

A	coefficient of the discretization equation, depending on equation
A	area of cross section/m^2
A, A′, A_0	circle center mark
a	coefficient of the discretization equation, depending on equation
a	radius of helically coiled tube/m
b	source term of discretization equation, depending on equation
c_p	heat capacity/kJ·(kg·K)$^{-1}$
D	hydraulic diameter of the tube /m
Dn	Dean number
d	tube diameter/m
$\boldsymbol{e}_{x'}$, $\boldsymbol{e}_{y'}$, $\boldsymbol{e}_{z'}$	unit vector along the coordinate x', y', z'
f	Fanning friction factor
H	tube pitch/m
h	convective heat transfer coefficient/W·(m^2·K)$^{-1}$
$\boldsymbol{i}, \boldsymbol{j}, \boldsymbol{k}$	unit vector along the coordinate x', y', z'/m
J	Jacobi factor
J^{n}	vorticity flux along the normal direction of cross section/s
$J^{\mathrm{n}}_{\mathrm{ABS}}$	absolute vorticity flux along the normal direction of cross section/s^{-1}
$J^{\mathrm{n}}_{\mathrm{ABS,V}}$	volumetrically averaged absolute vorticity flux /s^{-1}
K	tube pitch per unit rad/m
L	Axial length/m
L, M, N	grid number
$\boldsymbol{n}$	unit vector, normal direction of the cross section or wall surface
Nu	Nusselt number
p	static pressure/Pa
Pr	Prandtl number
q	heat flux/W·m^{-2}
Q	crossly averaged velocity component along the main flow direction/m·s^{-1}
R	radius of helically coiled tube center line/m
Re	Reynolds number
Re_{c}	Critical Reynolds number
r	radial coordinate/m
S	source term /depending on equation
S_{ad}	additional source term /depending on equation
Se	Reynolds number of secondary flow
T	temperature/K
U, V, W	contravariant velocity/m·s^{-1}
u', v', w'	velocity components along the coordinates x', y', z'/m·s^{-1}
u, v, w	velocity components along the coordinates x, y, z/m·s^{-1}
$\boldsymbol{v}$	velocity vector/m·s^{-1}
x, y, z	coordinates axes/m
x', y', z'	rotation axis/m

Greeks

α, β, γ	coefficient of the discretization equation
Γ	velocity loop/m^2·s^{-1}
Γ_ϕ	generalized diffusion coefficient, depending on equation
ζ, η, ξ	body-fitted coordinate axis/m
Θ	Dimensionless temperature
κ	dimensionless curvature
μ	dynamic viscosity/Pa·s
ρ	fluid density/kg·m^{-3}
τ	dimensionless torsion
ϕ	general variable, cross section angle, depending on equation
ω	vorticity component/s^{-1}
$\boldsymbol{\omega}$	vorticity vector/s^{-1}

Subscripts

ABS	absolute value
B	lower node
bulk	cross averaged value
E	east node
h	helically coiled tube
in	inlet
local	local value
m	averaged value
N	north node
out	outlet
P	major node
p	circumferential local value
S	south node
s	straight pipe
T	upper node
W	west node
w	wall

Superscript

′	corrected value
n	normal direction of cross section

transfer on the inner side surface of curved tube is deteriorated [4]. The results of Jamshidi et al. show that increasing the curvature radius of helically coiled tube can enhance the heat transfer in the tube, increase the pitch of helically coiled tube, and reduce the heat transfer coefficient in the tube [5]. Bersano and Falcone et al. [6] suggested that helically coiled tube could be used as the downcomer of the Bayonet tube heat exchanger in nuclear reactor. The heat transfer performance was improved by about 8%. Rabienataj and Abuzadeh et al. [7] showed that the local *Nu* number at the outer diameter is greater than that at the inner diameter. Zare and Heyhat et al. [8] showed that there is a larger temperature gradient near the outer wall than that of the inner wall. Jayakumar et al. [9] numerically investigated varying coil parameters such as diameter, tube pitch and pipe diameter and their influence on heat transfer for vertically oriented helical coils. Pawar et al. [10] studied the flow of Newtonian fluid and non-Newtonian fluid in helically coiled tube, obtained the correlation under laminar flow, which has better accuracy compared with the correlation in the literature. Han et al. [11] took heat transfer coefficient, flow resistance and entropy generation number as multi-objective functions, and adopted multi-objective parameter optimization method to study the optimal design of helically coiled tube heat exchanger. The optimal comprehensive performance can be obtained with the maximum heat transfer coefficient, minimum resistance and minimum entropy generation number as the objective function.

Ahadi and Abbassi et al. [12] carried out exergy analysis of laminar forced convection of nano-fluids in helically coiled tubes with uniform wall heat flux. With the increase of *Re* number and curvature, the thermal entropy production decreases and the frictional entropy production increases. Dimensionless pitch change has little effect on entropy generation. For Al_2O_3/water nano-fluid, Kumar et al. [13] observed that the overall heat transfer coefficient, heat transfer coefficient in the tube and experimental inner Nusselt number increased with the increase of the particle volume concentration and the increase of Dean number. Bahrehmand et al. [14] numerically investigated heat transfer characteristics of Al_2O_3 nano-fluid flow inside shell and helically coiled tube heat exchangers. For the same mass flow rate, the heat transfer rate of nano-fluid enhances noticeably compared to water and it increases marginally with the further increase in the nano-particle volume concentration. The research of Narrein [15] shows that Nusselt number is the highest when CuO water is used as nano-fluid. In addition, rotation can be used to improve the heat transfer rate. Huminic et al. [16] summarized the flow and heat transfer characteristics of conventional fluid and nano-fluid in helically coiled tube.

Some scholars have studied the flow and heat transfer in helically coiled tube with special structure, and further improved its heat transfer performance by changing the geometric morphology of the inner surface of helically coiled tube. Kumar and Solanki et al. [3] studied the heat transfer and pressure drop performance of helically coiled tubes with micro-fin under different structural parameters. Rainieri et al. [17] studied smooth helically coiled tube and corrugated helically coiled tube respectively, and analyzed the mechanism of heat transfer enhancement of the two kinds of tubes. Zheng et al. [18] studied the heat transfer performance of helically coiled tube with spherical protrusion. Secondary flow in tube is enhanced through the spherical protrusion. The tangential velocity is used to measure the secondary flow intensity. The two high tangential velocity regions in helically coiled tube are symmetrical about the center of the tube, and there is a low tangential velocity region inside the tube. There is a high temperature region inside helically coiled tube, and the two low temperature regions are symmetrically distributed on the upper and lower sides of helically coiled tube.

According to the available literature, helically coiled tube has greater heat transfer coefficient and higher pressure drop than straight tube. Secondary flow enforced by the centrifugal force is the main reason for the increases of heat transfer ability and pressure drop. The diameter ratio and pitch ratio have a great influence on secondary flow, thus on the average heat transfer coefficient. As indicated by Liu [19], *Dn* is a kind of parameter of measuring secondary flow intensity in helically coiled tube. With the increase of *Dn*, the heat transfer coefficient increases. The tangential velocity on the cross section of helically coiled tube can also be used to measure the secondary flow intensity [18]. Recently our group proposed one other parameter to specify the intensity of secondary flow [20, 21], which is absolute vorticity flux $J_{\mathrm{ABS}}^{\mathrm{n}}$ and its non-dimensional counter part. These show that there may be different descriptions for the secondary flow intensity in helically coiled circular tube. Thus, the description of secondary flow needs to be further studied to establish the relationship between the secondary flow intensity and heat transfer capability in helically coiled circular tube.

Based on these motivations, this paper tries to investigate the relationship absolute vorticity flux and heat transfer coefficient in helically coiled tubes, and to investigate the relationship between *Nu* and *Se* (normalized $J_{\mathrm{ABS}}^{\mathrm{n}}$, and named secondary flow Reynolds number). At the same time, the effects of curvature and torsion of helical tube on heat transfer are also studied.

2. Physical Model and Mathematical Formulation

A helically coiled circular tube, as displayed in Fig. 1, is formed through the motion of a base circle along a

helical path line, which is designated by tube diameter d, coil radius R, tube pitch H, here H=2$K\pi$. The tube geometry is well-determined by the curvature and torsion of the path line.

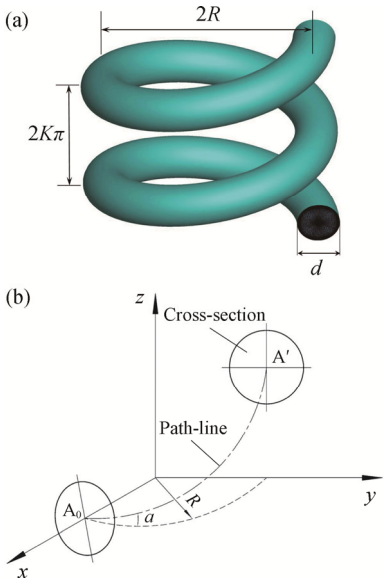

Fig. 1 Helically coiled tube and its reference coordinates system

The coordinates system used in this analysis is shown in Fig. 1(b). The helix angle of the tube axis is α. Point A_0 and A lies on the path line (viz. the tube axis), which are the centers of the starting cross-section and the middle cross-section, respectively. In order to guarantee the good orthogonality between the cross section and the tube axis, the solid line circles A_0 and A′ (they are cross section circles of the tube) are gained by rotation of the dashed circles A_0 and A′ (they are the original circles of those cross sections) which are parallel to the horizontal plane (the x-y plane), naturally, the angle contained by them is α.

The dimensionless curvature and dimensionless torsion are defined as:

$$\kappa = \frac{Rd/2}{R^2+K^2}, \quad \tau = \frac{Kd/2}{R^2+K^2} \tag{1}$$

To establish the mathematics model, viscous dissipation is neglected; the physical properties of fluid are constant; flow is laminar and steady flow; fluid is incompressible; fluid flow is fully developed both in fluid flow and heat transfer. Based on these assumptions, the governing equations could be written as follows.

Continuity equation:

$$\frac{\partial u}{\partial x}+\frac{\partial v}{\partial y}+\frac{\partial w}{\partial z}=0 \tag{2}$$

Momentum equation:

$$\frac{\partial}{\partial x_i}\left(\rho u_i u_k\right)=\frac{\partial}{\partial x_i}\left(\mu\frac{\partial u_k}{\partial x_i}\right)-\frac{\partial p}{\partial x_k} \qquad (k=1,2,3) \tag{3}$$

Energy equation:

$$\frac{\partial}{\partial x_i}\left(\rho c_p u_i T\right)=\frac{\partial}{\partial x_i}\left(\lambda\frac{\partial T}{\partial x_i}\right) \qquad (i=1,2,3) \tag{4}$$

where u, v, w are velocity components along x, y, z; p, ρ, μ are the pressure, density and dynamic viscosity of the fluid; T, c_p, λ are temperature, specific heat capacity and thermal conductivity, respectively.

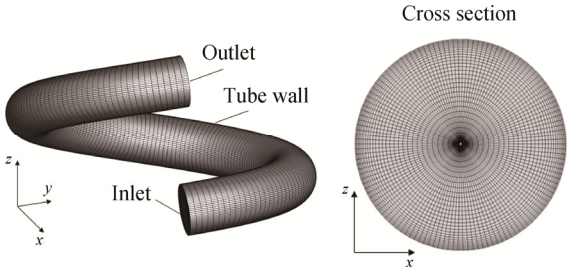

Fig. 2 Schematic view of the grid system of the computational domain

Considering usage of helically coiled tubes, generally their numbers of coiled turns are large; the entrance effect can be ignored. Therefore, the flow and heat transfer characteristics in helically coiled tube under the fully developed flow are studied. Considering the flow reaches the fully developed stage, the tube with the length having one cycle is selected as the computation domain, which is shown in Fig. 2. The boundary conditions are as follows: at the inlet and outlet cross section of the tube, the periodicity boundary condition is adopted.

$$\begin{aligned} u(x,y,z)\big|_{\text{in}} &= u(x,y,z)\big|_{\text{out}} \\ v(x,y,z)\big|_{\text{in}} &= v(x,y,z)\big|_{\text{out}} \\ w(x,y,z)\big|_{\text{in}} &= w(x,y,z)\big|_{\text{out}} \\ \Theta(x,y,z)\big|_{\text{in}} &= \Theta(x,y,z)\big|_{\text{out}} \end{aligned} \tag{5}$$

where the subscript "in" denotes the inlet, and "out" denotes the outlet of the tube. Θ is the dimensionless temperature defined as

$$\Theta=\frac{T(x,y,z)-T_{\text{w}}}{T_{\text{bulk}}-T_{\text{w}}} \tag{6}$$

where T_{w} is temperature of tube wall; T_{bulk} is the average temperature on a cross-section, defined as follows:

$$T_{\text{bulk}}=\frac{1}{A}\int_A u(x,y,z)T(x,y,z)\mathrm{d}A \tag{7}$$

On the tube wall, the no-slip condition for velocity and constant wall temperature are applied.

$$\begin{aligned} u(x,y,z)=0, \quad v(x,y,z)=0 \\ w(x,y,z)=0, \quad T(x,y,z)=T_{\text{w}} \end{aligned} \tag{8}$$

The Reynolds number is defined as

$$Re=\frac{\rho u_{\text{m}} D}{\mu} \tag{9}$$

where u_m is average axial velocity; D is hydraulic diameter of the tube.

This paper focuses on laminar flow, thereby, the axial variation is omitted and the pressure gradient is directly related to the friction factor as follows:

$$fRe = \frac{1}{4}\frac{2\Delta pD}{\rho u_m^2 L}Re \tag{10}$$

where Δp is pressure drop; L is the axial length of the tube; f is the Fanning friction factor that is $16/Re$ for a straight circular tube. We define a generalized Dean number as

$$Dn = Re\kappa^{1/2} = Re\left(\frac{Rd/2}{R^2+K^2}\right)^{1/2} \tag{11}$$

The crossly averaged velocity component along the main flow direction on the cross-section (x'-y' plane) is defined as

$$Q_h = \frac{1}{A}\int_A w'\mathrm{d}A \tag{12}$$

where A is the area of the cross-section; w' is the axial velocity.

The crossly averaged velocity component along the main flow direction of a straight tube with the same pressure $\Delta p/L$ gradient is defined as

$$\begin{aligned} Q_s &= \frac{1}{A}\int_0^a 2\pi r w'\mathrm{d}r \\ &= 2\pi\int_0^a \frac{1}{4\mu}\frac{\partial p}{\partial \zeta}\left(a^2-r^2\right)r\mathrm{d}r \\ &= \frac{\pi a^2\Delta p}{8\mu L} \end{aligned} \tag{13}$$

where L and a denote the length and the radius of the straight tube, respectively.

In order to obtain the effects of the secondary flow intensity on overall fluid flow and heat transfer characteristics, one definition of the intensity of secondary flow is necessary. Here the crossly averaged absolute vorticity flux on cross-section (x'-y' plane) is used to quantify the intensity of secondary flow locally.

$$J_{\mathrm{ABS}}^{\mathrm{n}} = \frac{1}{A}\iint_A \left|\omega^{\mathrm{n}}\right|\mathrm{d}A \tag{14a}$$

The intensity of secondary flow in total flow field is evaluated by

$$J_{\mathrm{ABS,V}}^{\mathrm{n}} = \frac{1}{V}\iint_V \left|\omega^{\mathrm{n}}\right|\mathrm{d}V \tag{14b}$$

The Nusselt numbers are calculated as

$$Nu_m = \left(h_m D\right)/\lambda_f \tag{15}$$

where Nu_m is the average Nu. h_m is determined as follows:

$$h_m = \frac{q_m}{\dfrac{\left(T_w - T_{\mathrm{bulk}}|_{\mathrm{in}}\right)-\left(T_w - T_{\mathrm{bulk}}|_{\mathrm{out}}\right)}{\ln\left[\left(T_w - T_{\mathrm{bulk}}|_{\mathrm{in}}\right)/\left(T_w - T_{\mathrm{bulk}}|_{\mathrm{out}}\right)\right]}} \tag{16}$$

The averaged q_m is obtained from the local heat flux on the tube wall and it is calculated by the Fourier's law, then it is averaged over total circular tube surface.

In fact, the velocity components are the projection of velocity vector $\boldsymbol{v}$ along each coordinate. Thus, in order to obtain the velocity component along the coordinate y', z', the unit normal vector of cross-section and the unit vectors along the coordinate y', z' should be given. Here, the unit vector normal to the iso-surface of a function and directing to the larger value of this function can be defined as follows:

$$n^{(f)} = \frac{\nabla f}{|\nabla f|} \tag{17a}$$

and if the function is $f=\zeta$ (the coordinate of tube axial), we get

$$n^{(\zeta)} = \frac{\nabla \zeta}{|\nabla \zeta|} = \frac{\gamma_1 \boldsymbol{i}+\gamma_2 \boldsymbol{j}+\gamma_3 \boldsymbol{k}}{\sqrt{\gamma_1^2+\gamma_2^2+\gamma_3^2}} \tag{17b}$$

where $\boldsymbol{i}$, $\boldsymbol{j}$, $\boldsymbol{k}$ denote the unit vector along the coordinate x, y, z. Thus

$$\boldsymbol{e}_{z'} = -\boldsymbol{n}^{(\zeta)} = -\frac{\gamma_1 \boldsymbol{i}+\gamma_2 \boldsymbol{j}+\gamma_3 \boldsymbol{k}}{\sqrt{\gamma_1^2+\gamma_2^2+\gamma_3^2}} \tag{17c}$$

$$\begin{cases} \gamma_1 = y_\xi z_\eta - z_\xi y_\eta \\ \gamma_2 = z_\xi x_\eta - x_\xi z_\eta \\ \gamma_3 = x_\xi y_\eta - y_\xi x_\eta \end{cases} \tag{17d}$$

The secondary flow induced in helically coiled tubes can be described as multiple superposition of vortexes. The intensity of vortex is mathematically defined as

$$\boldsymbol{\omega} = \nabla \times \boldsymbol{v} = \omega_x \boldsymbol{i} + \omega_y \boldsymbol{j} + \omega_z \boldsymbol{k} \tag{18a}$$

where, ω_x, ω_y and ω_z are defined as follows:

$$\omega_x = \frac{\partial w}{\partial y} - \frac{\partial v}{\partial z}, \quad \omega_y = \frac{\partial u}{\partial z} - \frac{\partial w}{\partial x}, \quad \omega_z = \frac{\partial v}{\partial x} - \frac{\partial u}{\partial y} \tag{18b}$$

The vorticity ω^{n} along axial direction z' of Eq. (18) is defined as

$$\begin{aligned} \omega^{\mathrm{n}} &= \boldsymbol{\omega}\cdot\boldsymbol{e}_{z'} \\ &= \left(\omega_x \boldsymbol{e}_{x'} + \omega_y \boldsymbol{e}_{y'} + \omega_z \boldsymbol{e}_{z'}\right)\times\left(\frac{\gamma_1}{\sqrt{\gamma}}\boldsymbol{i} + \frac{\gamma_2}{\sqrt{\gamma}}\boldsymbol{j} + \frac{\gamma_3}{\sqrt{\gamma}}\boldsymbol{k}\right) \\ &= \frac{\gamma_1}{\sqrt{\gamma}}\omega_x + \frac{\gamma_2}{\sqrt{\gamma}}\omega_y + \frac{\gamma_3}{\sqrt{\gamma}}\omega_z \end{aligned} \tag{19}$$

Thus, the absolute vorticity flux defined in Eq. (14) can be calculated as

$$J_{\mathrm{ABS}}^{n} = \frac{1}{A}\iint_A \left|\frac{\gamma_1}{\sqrt{\gamma}}\omega_x + \frac{\gamma_2}{\sqrt{\gamma}}\omega_y + \frac{\gamma_3}{\sqrt{\gamma}}\omega_z\right|\mathrm{d}A \tag{20}$$

and

$$J_{\mathrm{ABS},V}^{n} = \frac{1}{V}\iint_V \frac{1}{\sqrt{\gamma}}\left|\gamma_1\omega_x + \gamma_2\omega_y + \gamma_3\omega_z\right|\mathrm{d}V \tag{21}$$

The secondary flow Reynolds number is used to describe the secondary flow intensity in many cases, such

as in twisted tube [22–24]. The secondary flow Reynolds number is defined as [25]:

$$Se = \frac{\rho\left(D \times J^{n}_{ABS,V}\right)D}{\mu} = \frac{\rho D^2}{\mu} \times J^{n}_{ABS,V} \tag{22}$$

where $J^{n}_{ABS,V}$ is the volumetrically averaged absolute vorticity flux, which is averaged in total fluid flow region. Se is secondary flow Reynolds number; ρ is the density of the fluid; D is the hydraulic diameter of the tube; μ is kinetic viscosity.

3. Numerical Method and Validation

3.1 Numerical method

The simulation domain in physical space (x, y, z) coordinates is transformed into a rectangular domain in the computational space (ξ, η, ζ) coordinates by using the transfinite interpolation algebraic method [26, 27].

The governing equations show in Eqs. (2)–(4) are transferred into computational space:

$$\frac{\partial(\rho U)}{\partial \xi} + \frac{\partial(\rho V)}{\partial \eta} + \frac{\partial(\rho W)}{\partial \zeta} = 0 \tag{23}$$

$$\frac{\partial(\rho U\phi)}{\partial \xi} + \frac{\partial(\rho V\phi)}{\partial \eta} + \frac{\partial(\rho W\phi)}{\partial \zeta} = \frac{\partial}{\partial \xi}\left(\frac{\alpha}{J}\Gamma^{\phi}\frac{\partial \phi}{\partial \xi}\right) + \frac{\partial}{\partial \eta}\left(\frac{\beta}{J}\Gamma^{\phi}\frac{\partial \phi}{\partial \eta}\right) + \frac{\partial}{\partial \zeta}\left(\frac{\gamma}{J}\Gamma^{\phi}\frac{\partial \phi}{\partial \zeta}\right) + JS \tag{24}$$

where U, V, W are contravariant velocity components along (ξ, η, ζ), respectively, i.e.

$$\begin{aligned} U &= \alpha_1 u + \alpha_2 v + \alpha_3 w \\ V &= \beta_1 u + \beta_2 v + \beta_3 w \\ W &= \gamma_1 u + \gamma_2 v + \gamma_3 w \end{aligned} \tag{25}$$

They are discretized using the control volume method. The power scheme is used to discretize the convective terms, while the second order central difference schemes are employed for the viscous and source terms. SIMPLE algorithm is used to couple the velocity and pressure [28]. The discretized form of Eq. (24) can be obtained as follows.

$$\begin{aligned} a_P\varphi_P = {} & a_E\varphi_E + a_W\varphi_W + a_N\varphi_N + a_S\varphi_S \\ & + a_T\varphi_T + a_B\varphi_B + b + S_{ad} \end{aligned} \tag{26}$$

The set of many equations are solved by TDMA (Tridiagonal matrix method).

3.2 Validation of numerical method

The structured grid system of the computational domain is schematically shown in Fig. 2. The grid independence test has been successfully carried out for different grid sizes. Five different grid arrangements (x-direction grid number L, y-direction grid number M, axial-direction grid number N) have been considered.

Table 1 gives the comparison of numerical results under the following conditions: 65×15×80, 65×21×150, 95×21×150, 131×31×150, 131×31×250 for Dn=500.0, κ=0.2484, τ=0.0198; the deviation values of $J^{n}_{ABS,V}$, Nu_m, f_h/f_s, Q_h/Q_s and fRe calculated by the two largest grids are less than 5%. The Effect of the grid arrangements on the dimensionless axial velocity along ζ is shown in Fig. 3. The axial velocity has little difference in different grid arrangements. Considering the good economy and accuracy of calculations, the results presented in this paper are based on the calculations of the 131×31×150 grid arrangement.

The numerical results are verified by comparison with the results in the previous literature. The pressure gradient fRe is obtained by numerical simulation of helically coiled circular tubes with different structural parameters. Compared with the results of Liu and Masliyah [19], it is found that the maximum error of pressure gradient is 8.52% under different Dn numbers.

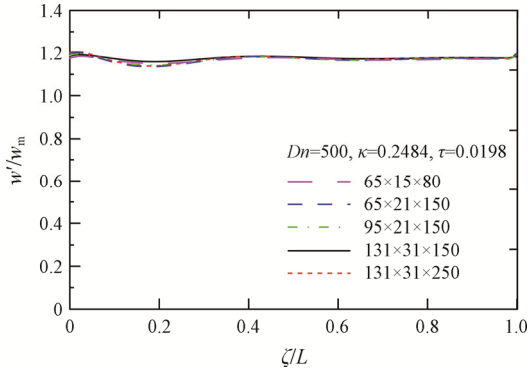

Fig. 3 Effect of the grid arrangements on the dimensionless axial velocity along ζ

Table 1 Comparisons of the results for the different grid arrangements

$L \times M \times N$	J^{n}_{ABS}	Nu_m	f_h/f_s	Q_h/Q_s	fRe	% Divergence of J^{n}_{ABS}
65×15×80	7020.34	17.910	3.447	0.290	55.16	–5.75
65×21×150	7321.95	17.944	3.189	0.314	51.02	–1.70
95×21×150	7318.81	18.060	3.183	0.314	50.93	–1.74
131×31×150	7459.75	18.206	3.181	0.314	50.90	0.15
131×31×250	7448.33	18.284	3.059	0.327	48.95	0.00

Fig. 4 shows that the numerical method can well simulate the flow in a helically coiled circular tube.

At the same time, the heat transfer in helically coiled circular tube is also verified. Schmidt et al. [1] proposed correlations suitable for laminar flow and turbulence in helical tubes. In the range of laminar flow:

$$Nu = 3.65 + 0.08 \times \left[1 + 0.8\left(r/R\right)^{0.9}\right] \times Re^{\left[0.5+0.2903\left(r/R\right)^{0.194}\right]} \times Pr^{1/3} \quad (27)$$

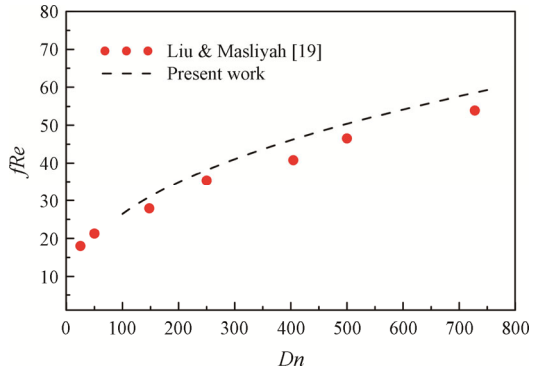

Fig. 4 The comparison of fully developed dimensionless axial velocity on x'-z' plane

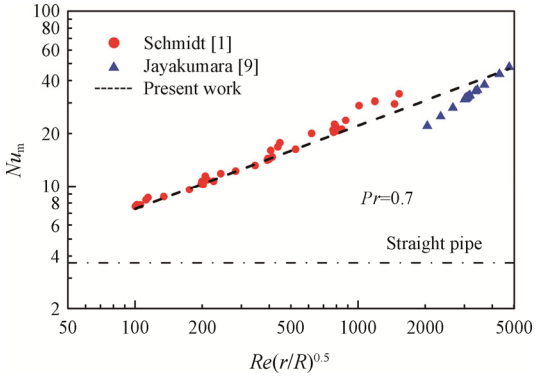

Fig. 5 The comparison of average Nusselt number with literature

The Reynolds number Re ranges from 100 to the critical Reynolds number Re_c.

$$Re_c = 2300 \times \left[1 + 8.6\left(r/R\right)^{0.45}\right] \quad (28)$$

For the large Reynolds number in the laminar flow range, Jayakumara et al. [9] established the correlation of heat transfer coefficient in helically coiled tube according to the experimental results.

$$Nu = 0.025 \times Dn^{0.9112} \times Pr^{0.4}, \quad 2000 < Dn < 12\,000 \quad (29)$$

where Dn is the Dean number, which is defined as:

$$Dn = Re \times \left(r/R\right)^{0.5} \quad (30)$$

The numerical method used in this paper is compared with the correlation in the literature, and the results are shown in Fig. 5. Due to the different application ranges of the above correlation, when the Dn number is less than 2000, the correlation proposed by Schmidt is in good agreement with the numerical results. When the Dn number is greater than 2000, the correlation obtained by Jayakumara [9] is in good agreement with the numerical results. According to the comparisons above, we could claim that the code is valid.

3.3 Studied cases

In order to obtain useful results, the situation of helically coiled circular tube with different structural parameters under different Dn numbers was studied. In the previous literature, only helically coiled circular tube with small torsion has been studied. In order to easy find parametric effects on fluid flow and heat transfer characteristics geometrical sizes shown in Table 2 are designed. There are 28 structures in total, of which the value of dimensionless curvature ranges from 0.01 to 0.52; the value range of dimensionless torsion is 0.018 to 0.289; the value range of Dn number is 100 to 3000. The range of structural parameters and Dn number in this study is relatively large.

Table 2 The parameters of the studied cases

Case No.	κ	τ	Case No.	κ	τ	Case No.	κ	τ
1	0.52	0.289	11	0.5	0.144	21	0.11	0.036
2	0.34	0.289	12	0.45	0.072	22	0.04	0.036
3	0.16	0.289	13	0.37	0.072	23	0.01	0.036
4	0.44	0.222	14	0.29	0.072	24	0.23	0.018
5	0.31	0.222	15	0.21	0.072	25	0.18	0.018
6	0.18	0.222	16	0.13	0.072	26	0.13	0.018
7	0.5	0.144	17	0.05	0.072	27	0.08	0.018
8	0.38	0.144	18	0.32	0.036	28	0.04	0.018
9	0.26	0.144	19	0.25	0.036			
10	0.14	0.144	20	0.18	0.036			

4. Numerical Results and Discussion

4.1 The velocity, J^{n}_{ABS} and temperature distributions on x'-y' cross section

Fig. 6 depicts the secondary flow velocity fields under different *Dn* number. For smaller Dean number, the distribution of the secondary flow velocity is uniform for the effect of the radial force on the fluid flow is weak. As seen in Fig. 6(a), two counter rotation vortexes locate near the central region symmetrically with respect to x'-axis on the cross-section, and the secondary flow velocity is larger than other place meaning the secondary flow is also strong. For these conditions, the vortexes are far away from the tube wall, so the enhanced effect on heat or mass transfer is not obvious. However, with increasing of *Dn* number, as displayed in Fig. 6(d), the secondary flow becomes more intense; the vortexes move towards the tube wall. This phenomenon is benefit for heat or mass enhancement because it leads the intermixing of fluid between the region of interior and the wall side.

As defined in Eq. (14), J^{n}_{ABS} is absolute vorticity along the main flow on the cross section x'-y', and J^{n}_{ABS} is just the value of $|\omega^{n}|$. Fig. 7 depicts the distribution of the absolute vorticity on the same cross-section under different *Dn* number. As observed in the figures, for one location, the value of J^{n}_{ABS} represents the intensity of the secondary flow; namely they are one-to-one correspondence: the larger secondary flow velocity corresponds to the larger J^{n}_{ABS}. It can be seen from the figure that when the *Dn* number is small, the maximum value of absolute vorticity flux is also small. The region

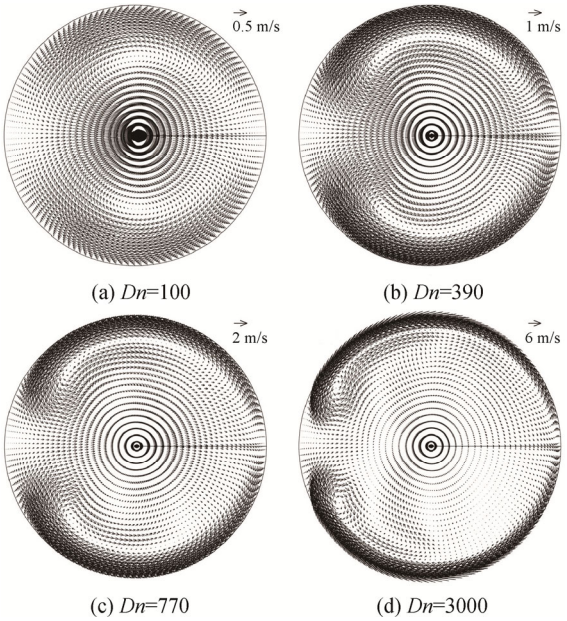

(a) *Dn*=100 (b) *Dn*=390

(c) *Dn*=770 (d) *Dn*=3000

Fig. 6 The velocity distribution of cross section at different *Dn* numbers

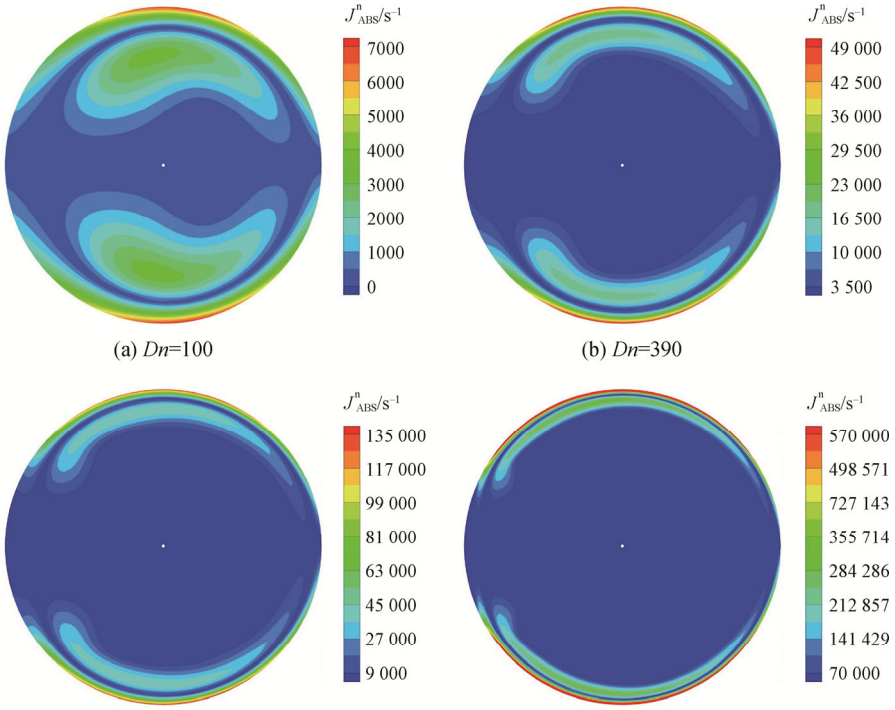

(a) *Dn*=100 (b) *Dn*=390

(c) *Dn*=770 (d) *Dn*=3000

Fig. 7 The J^{n}_{ABS} distribution of cross section at different *Dn* numbers

with large absolute vorticity flux is in the position of a pair of symmetrical vortices. As *Dn* number increases, the value of J^{n}_{ABS} on the cross section also increases. The region with large absolute vorticity flux moves towards the upper and lower walls of the tube.

Fig. 8 shows the cloud diagram of the dimensionless temperature Θ distribution on the cross section of helically coiled circular tube with fixed structure at different *Dn* numbers. As can be seen from Fig. 8, the regions with large dimensionless temperature values are distributed outer side of the tube. As *Dn* number increases, the region with large dimensionless temperature values is closer to the tube wall and symmetrically distributed along the horizontal line. The reason is that with the increase of flow velocity, enhanced secondary flow leads to more obvious fluid mixing on the cross section, so that the temperature on the section tends to be uniform.

4.2 Relationship between $J^{n}_{ABS,V}$ and *Re*

Absolute vorticity flux $J^{n}_{ABS,V}$ is used to describe the intensity of secondary flow on the cross section. As can be seen from Fig. 9, for the same structure, the absolute vorticity flux increases with the increase of *Re* number. The greater the flow velocity in helically coiled circular tube, the greater the centrifugal force and viscous shear stress of the fluid, and the greater the secondary flow intensity. For tubes with different structural parameters, even if the *Re* number is the same, there are different secondary flow intensity. In the legend, the first number after the symbol is the dimensionless curvature κ, and the second number is the dimensionless torsion τ.

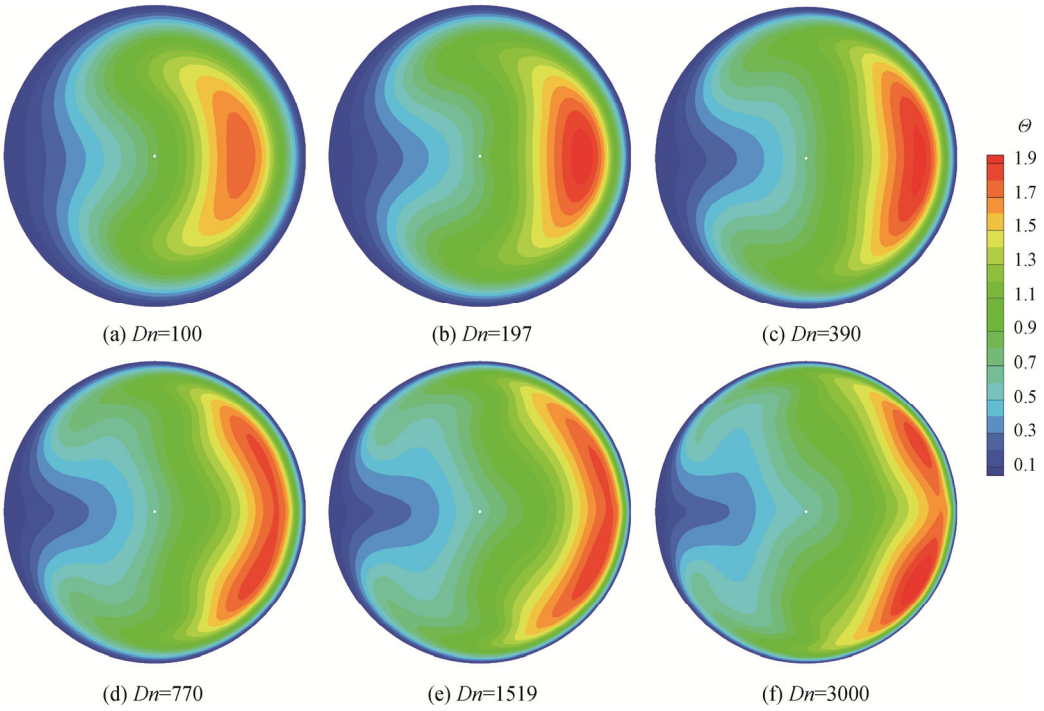

Fig. 8 The dimensionless temperature distribution at different *Dn* numbers

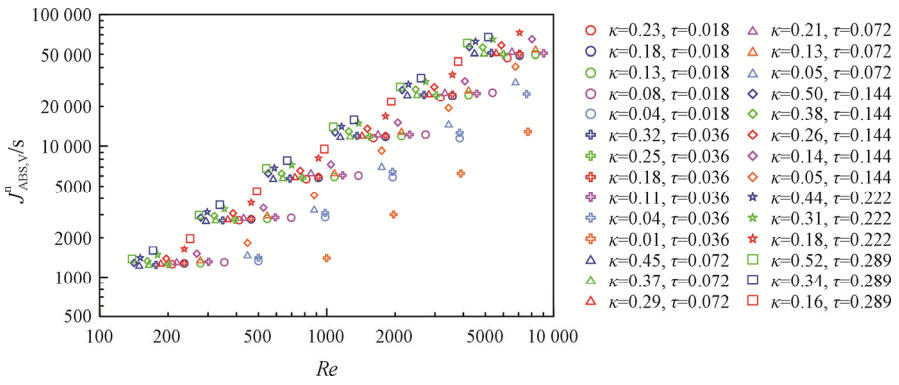

Fig. 9 Relationship between $J^{n}_{ABS,V}$ and *Re*, *Pr*=0.7

4.3 Relationship between $J^{n}_{ABS,V}$ and *Dn*

Dn number is used to describe the flow in helically coiled circular tube, which is a combination of *Re* number and dimensionless curvature, so *Dn* number and absolute vorticity flux $J^{n}_{ABS,V}$ show good consistency. As can be seen from Fig. 10, when the *Dn* number increases, the absolute vorticity flux increases. The absolute vorticity flux increases exponentially with *Dn* number.

4.4 Relationship between *Se* and *Dn*

It can be seen from Eq. (21) that $J^{n}_{ABS,V}$ can be obtained from the secondary flow velocity field on the cross section, but it is not a dimensionless parameter. These characteristics are disadvantage to data processing. Secondary flow Reynolds number *Se* is a dimensionless number. *Se* includes the effects of the kinds of fluid and the diameters of tubes.

Dn number includes Reynolds number and dimensionless structure parameters, and *Se* number is a dimensionless number calculated from the secondary flow velocity field on the cross section. The *Se* number can be a constant for different tube geometric parameters. Fig. 11 shows the relationship between *Se* and *Dn*. As expected, helically coiled tubes with different structural parameters have almost the same *Se* number for a given *Dn* number. Based on the present result, the quantitative relationship between *Se* and *Dn* is obtained.

$$Se = 4.5534Dn - 155.18$$
$$100 \le Dn \le 3000,\ 0.01 \le \kappa \le 0.52,\ 0.018 \le \tau \le 0.289,\ Pr = 0.7 \quad (31)$$

The maximum fitting error is about 22.8%.

There is a linear relationship between *Se* and *Dn*, which further proves the universality of the dimensionless parameter *Se*. In some cases, *Se* number can be used to indicate the physical meaning of *Dn* number.

4.5 Relationship between h_m and $J^{n}_{ABS,V}$

Fig. 12 depicts the relationship between heat transfer coefficient h_m and absolute vorticity flux $J^{n}_{ABS,V}$ for same tube diameters. It is found that h_m increases with increasing of $J^{n}_{ABS,V}$. The greater the absolute vorticity flux is, the greater the secondary flow intensity is. Secondary flow on the cross section strengthens the heat transfer at the tube wall and makes it have a larger heat transfer coefficient. Most cases show high correlation between heat transfer coefficient and absolute vorticity flux. When the absolute vorticity flux is large, some points are scattered.

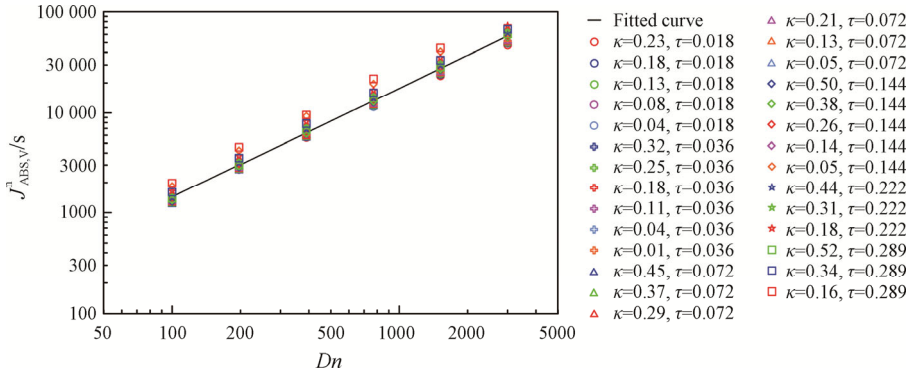

Fig. 10 Relationship between $J^{n}_{ABS,V}$ and *Dn*, *Pr*=0.7

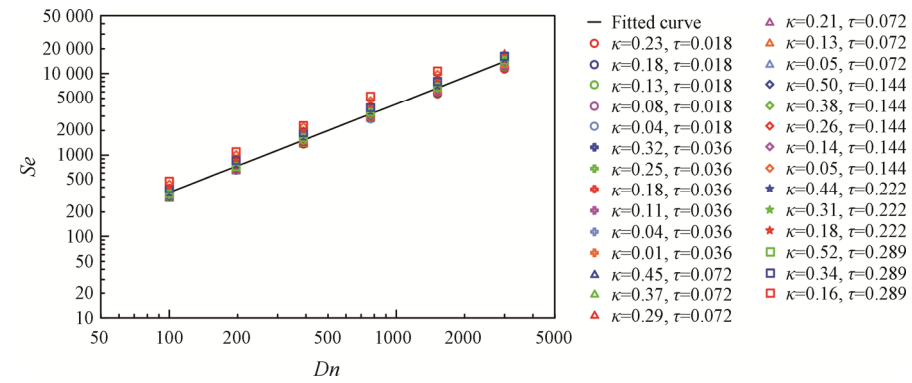

Fig. 11 *Se* dependence on *Dn*, *Pr*=0.7, *Dn*=100–3000

4.6 Relationship between Nu_m and Se

The relationship between Nu_m and Se is shown in Fig. 13. From the plot, we can find that the overall intensity of convective heat transfer in helically coiled tube with uniform wall temperature is invariable for a fixed secondary flow Re number despite of the changes of curvature and torsion. A correlation between the Nu number and Se number, dimensionless curvature, and dimensionless torsion is obtained using least square analysis. The coefficient of Nu_m and Se can be expressed by the following formulation.

$$Nu_m = 0.5040 Se^{0.455\,1} \kappa^{0.047\,36} \tau^{-0.066\,28},$$
$$100 \le Dn \le 3000,\ 0.01 \le \kappa \le 0.52,\ 0.018 \le \tau \le 0.289,\ Pr = 0.7 \quad (32)$$

It can be seen from Eq. (32) that the exponent of dimensionless curvature and dimensionless torsion are close to zero, and the difference of secondary flow intensity caused by different structural parameters can be described by Se number. Eq. (32) shows the relationship between the secondary flow intensity Se number and Nu number. The maximum fitting error of Eq. (32) is about 10%.

4.7 Relationship between Nu_m and Dn

For fully developed flow, Nu_m of each cross-section are constant that for a given Dn, and it increases with increasing of Dn. The distribution of averaged Nu number has nearly the same tendency with the cross-section averaged absolute vorticity flux along the mainstream.

The relationship between the overall Nu_m number and the Dn number for different tube geometries is shown in Fig. 14. The fitting formula for Nu_m number as well as and dimensionless curvature, dimensionless torsion and Dn number has been got. The relationship is shown in Eq. (33).

$$Nu_m = 0.8001 Dn^{0.497\,5} \kappa^{0.007\,29} \tau^{-0.003\,452},$$
$$100 \le Dn \le 3000,\ 0.01 \le \kappa \le 0.52,\ 0.018 \le \tau \le 0.289,\ Pr = 0.7 \quad (33)$$

It can be seen that the exponents of dimensionless curvature and dimensionless torsion are close to zero, which means Nu_m number is related to Dn number, and which includes the influence of curvature and torsion. There is a quantitative relationship between Nu_m and Dn. It is that Nu_m exponentially increases with increasing of Dn. The maximum fitting error of Eq. (33) is 12.6%.

According to Eqs. (32) and (33), it can be seen that the secondary flow intensity in helically coiled circular tube can be described by Dn number or Se number, and they are exponential relationship with Nu_m number.

4.8 Relationship between Nu_m and Re

Dean number only depends on Re for a given tube geometry. For secondary flow induced in tube flow, Re

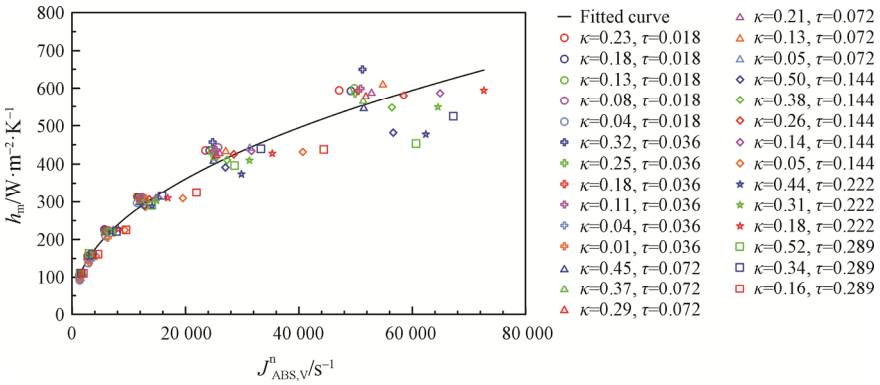

Fig. 12 Relationship between the heat transfer coefficient and $J^n_{ABS,V}$, Pr=0.7

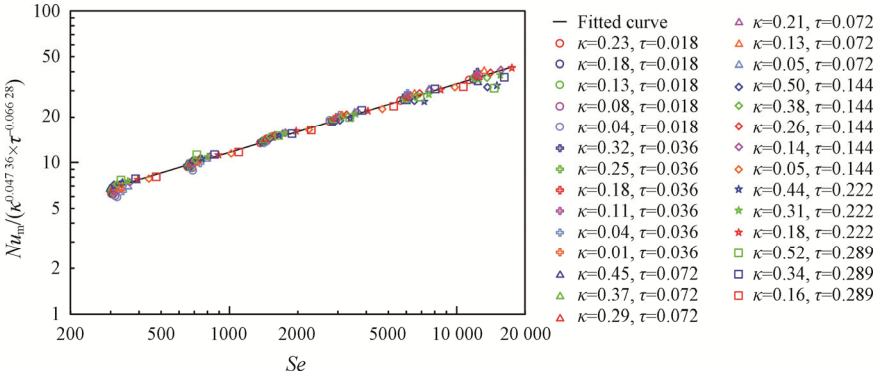

Fig. 13 Nu_m dependence on Se under different tube geometries, Pr=0.7

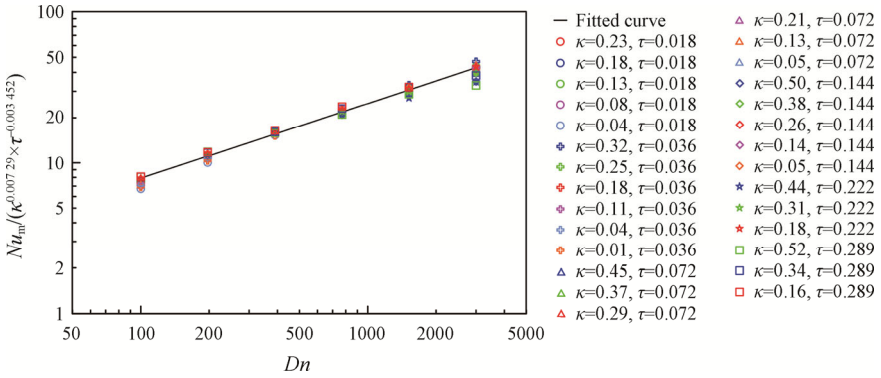

Fig. 14 Nu_m dependence on Dn under different tube geometries, Pr=0.7

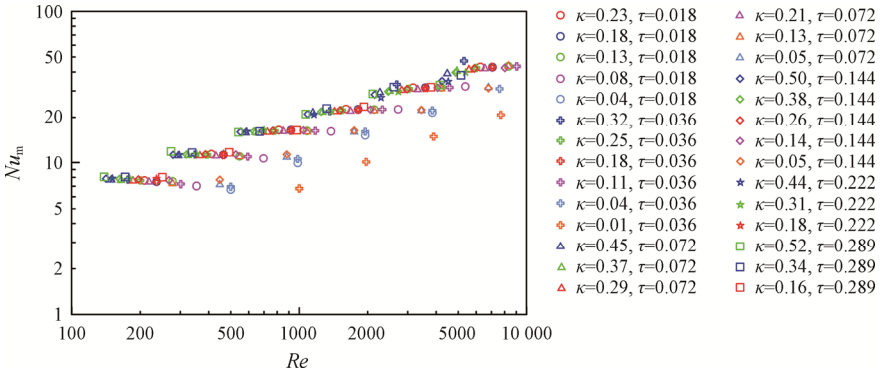

Fig. 15 Nu_m dependence on Re, Pr=0.7

represents the unstable extent and the intensity of secondary flow. Thus, a larger Re should generate stronger secondary flow, and a larger Nu_m should be obtained as well. The dependence of Nu_m on Re is shown in Fig. 15. Nu_m increases exponentially with the increasing of Re.

At the same Re number, helically coiled tubes with different structural parameters have different Nu_m numbers. It shows that the flow in helically coiled tube is very different from that in straight tube. The flow in helically coiled tube is affected by the structural parameters of the tube. It can be seen from the figure that a tube with large dimensionless curvature can have a large Nu number at a small Re.

4.9 Effect of dimensionless curvature κ on Nu_m

In order to investigate the effect of dimensionless curvature on the convective heat transfer characteristic in helically coiled tubes, some cases with the same dimensionless torsion are selected for comparative analysis. The Nu_m variation with Re under the fixed dimensionless torsion and different dimensionless curvature is presented in Fig. 15. Even if the dimensionless torsion is the same, the Nu_m number corresponding to different dimensionless curvature is different. The smaller the dimensionless curvature, the smaller the Nu_m number. That is, the smaller the dimensionless curvature is, the closer helically coiled tube is to the straight tube, and the worse the heat transfer performance. It can be concluded that under the same Re, the larger the dimensionless curvature, the better the corresponding heat transfer performance.

4.10 Effect of dimensionless torsion τ on Nu_m

Similarly, in order to investigate the effect of dimensionless torsion on the flow in helically coiled tubes, some cases with the same dimensionless curvature are selected for comparative analysis. As we known that for a toroidal tube the characteristic of flow is symmetrical with respect to the horizon plane of symmetry. But for a helically coiled tube, the force from the tube wall will apply twisting moment to the flow, and thus the flow field on cross-section will be not symmetrical with respect to the horizon plane of symmetry any more.

It can be seen from Fig. 15 that Nu_m changes little with the change of the dimensionless torsion when the dimensionless curvature is the same. It means that the influence of torsion under the same curvature and Re number is so little that the intensity of heat transfer enhancement changes little.

4.11 Relationship between f_h and Re

The relationship between the friction factor f_h and Re is shown in Fig. 16. It can be seen from Fig. 16 that the friction factor decreases with the increase of Re number, which is consistent with the change law of the friction

factor in the straight tube. In the laminar flow range, the friction factor of the straight tube is 16/*Re*, and the friction factor of helically coiled tube is obviously larger than that of the straight tube. The friction factor curves of helically coiled tubes with different structures have different slopes, which indicates that the structure of helically coiled tubes makes the flow in the tube more complicated than that in straight tubes, and its structural parameters have a great impact on the friction factor. It is not enough to use *Re* number to characterize the flow in helically coiled tube, and it is better to use *Dn* number and *Se* number.

4.12 Relationship between f_h and $J^n_{ABS,V}$

It can be seen from Fig. 17 that the friction factor of the tubes with the same structure parameters decreases with the increase of absolute vorticity flux. From the previous analysis, it can be concluded that the greater the velocity, the greater the absolute vorticity flux. The friction factor decreases with the increase of flow velocity, and is less than 0.25. Tubes with smaller dimensionless curvature has lower friction factor. The reason is that the less obvious the bending degree of the tube, the smaller the flow resistance of the tube.

4.13 Relationship between *fRe* and *Dn*

Fig. 18 show the relationship between *fRe* and *Dn*. The pressure gradient *fRe* increases with the increase of *Dn* number. When the *Dn* number is small, the pressure gradients of the tubes with different structures have little difference. When the *Dn* number is large, the pressure gradients of tubes with different structures have great difference. At the same time, it can be seen that the case with large dimensionless curvature has a large pressure gradient. The larger the curvature, the smaller the bending radius and the more obvious the change of velocity in the tube.

The relationship between pressure gradient *fRe* and *Dn* number, dimensionless curvature, and dimensionless torsion is obtained. The maximum fitting error of Eq. (34) is less than 20%.

$$fRe = 4.3197Dn^{0.4449}\kappa^{0.0958}\tau^{0.038},$$
$$100 \le Dn \le 3000, 0.01 \le \kappa \le 0.52, \quad (34)$$
$$0.018 \le \tau \le 0.289, Pr = 0.7$$

It can be seen from Eq. (34) that κ and τ have a great influence on the pressure gradient. The formula can be used to predict the axial pressure gradient in helically coiled tube when the *Dn* number is known.

4.14 Relationship between *fRe* and *Se*

The pressure gradient *fRe* is related to the friction factor, and its relationship is shown in Eq. (10). Fig. 19 displayed the effect of *Se* on pressure gradient *fRe*. In general, the pressure gradient increases with the increase of *Se* number. For the same structure, higher velocity will

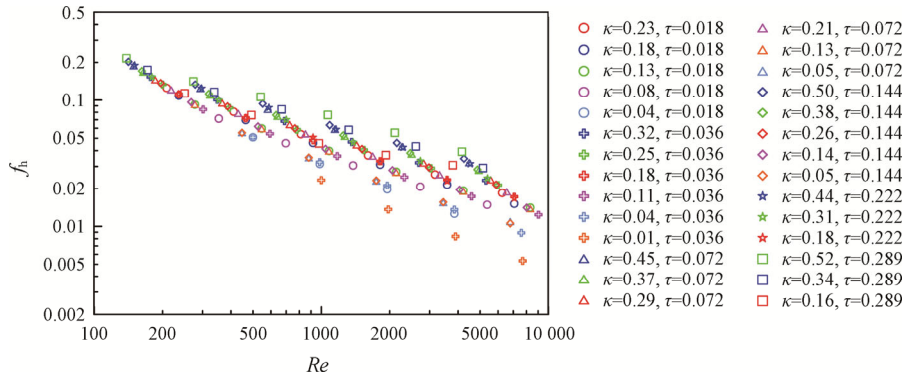

Fig. 16 Relationship between the friction factor and *Re*, *Pr*=0.7

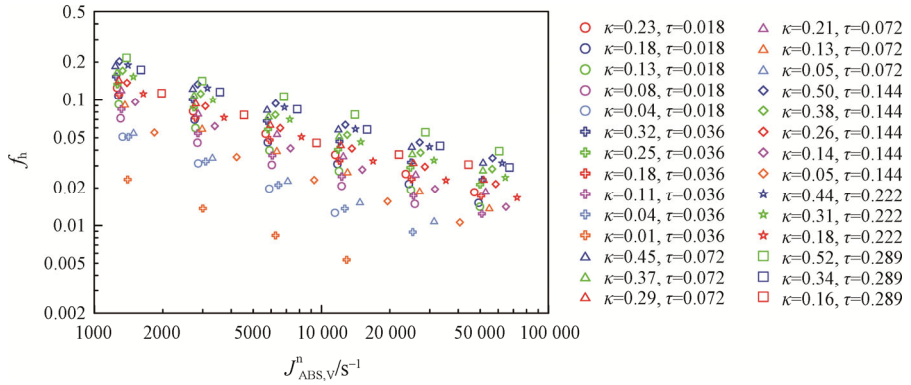

Fig. 17 Relationship between the friction factor and $J^n_{ABS,V}$, *Pr*=0.7

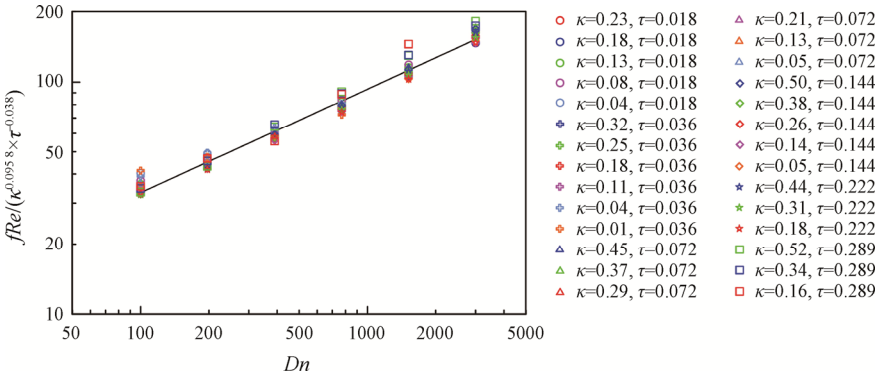

Fig. 18 Relationship between *fRe* and *Dn*, *Pr*=0.7

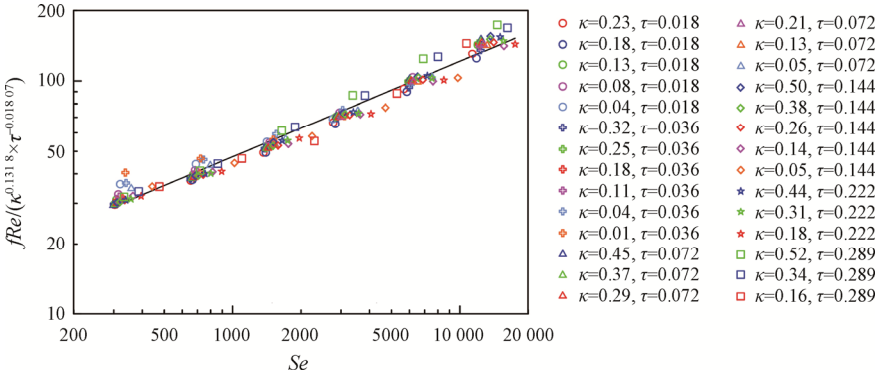

Fig. 19 Effect of *Se* on *fRe* under various *Dn* and tubes geometries

induce stronger secondary flow and cause greater pressure loss. However, there is no one-to-one correspondence between pressure gradient and *Se* number. The relationship between *fRe* and *Se* number is shown by Eq. (35).

$$fRe = 2.8844Se^{0.4058}\kappa^{0.1318}\tau^{-0.018\ 07},$$
$$100 \le Dn \le 3000,\ 0.01 \le \kappa \le 0.52, \qquad (35)$$
$$0.018 \le \tau \le 0.289,\ Pr = 0.7$$

The *Se* number describes the secondary flow intensity on the cross section, while the pressure gradient indicates the pressure loss along the tube axis. When the *Se* number is small, the pressure gradient in helically coiled tube with different structural parameters has a good correlation with the *Se* number. When the *Se* number is large, the correlation between the pressure gradient in helically coiled tube and the *Se* number is loose. The maximum fitting error of Eq. (35) is less than 20%.

5. Conclusions

Secondary flow in fully developed incompressible laminar flow of Newtonian fluid in helically coiled tubes with constant circular cross section, arbitrary torsion and arbitrary curvature is numerically studied. The absolute vorticity flux $J^{n}_{ABS,V}$ and its dimensionless parameter the secondary flow Reynolds number are used to describe the intensity of secondary flow. The relationships between the intensity of secondary flow and the fluid flow and heat transfer characteristics are studied. The outcome of numerical results can be summarized as follows.

In helically coiled tube, the intensity of secondary flow can be predicated by a given *Se* regardless of the tube geometry, *Re* number and *Dn* number.

The distribution of the averaged Nusselt number has nearly the same tendency with the cross-section averaged absolute vorticity flux in the main flow direction. With increase of the absolute vorticity flux, the value of the span averaged Nusselt number enlarges by exponential way. The overall convective heat transfer intensity in helically coiled tube with uniform wall temperature changes little for a fixed *Se* despite of the changes in tube geometry. The secondary flow intensity in helically coiled circular tube can be described by *Dn* number or *Se* number, and they are exponential relationship with *Nu* number.

The *Nu* of helically coiled tubes increases obviously as the dimensionless curvature increases for the fixed dimensionless torsion and Reynolds number. The dimensionless curvature is significant in controlling the degree of heat transfer in helically coiled tubes. *Nu* changes little as the dimensionless torsion changes for the fixed dimensionless curvature and Reynolds number.

Acknowledgments

This work is supported by the National Natural Science Foundation of China (No. 51776093, No. 52066009), Transformation of S&T achievements in Universities of Gansu Province of China (No. 2019C-06), Major Special Projects of Gansu Province of China (21ZD4GA027), Young Scientists Fund of Lanzhou Jiaotong University (2020038).

References

[1] Schmidt D.I.E.F., Wrmeübergang und druckverlust in rohrschlangen. Chemie Ingenieur Technik, 1967, 39(13): 781–789.

[2] Ko T.H., Ting K., Optimal Reynolds number for the fully developed laminar forced convection in a helical coiled tube. Energy, 2004, 31(12): 2142–2152.

[3] Kumar E.P., Solanki A.K., Kumar M., Numerical investigation of heat transfer and pressure drop characteristics in the micro-fin helically coiled tubes. Applied Thermal Engineering, 2021, 182: 116093.

[4] Liberto M.D., Ciofalo M., A study of turbulent heat transfer in curved pipes by numerical simulation. International Journal of Heat & Mass Transfer, 2013, 59: 112–125.

[5] Jamshidi N., Farhadi M., Ganji D.D., Sedighi K., Experimental analysis of heat transfer enhancement in shell and helical tube heat exchangers. Applied Thermal Engineering, 2013, 51: 644–652.

[6] Bersano A., Falcone N., Bertani C., Conceptual design of a bayonet tube steam generator with heat transfer enhancement using a helical coiled downcomer. Progress in Nuclear Energy, 2018, 108: 243–252.

[7] Rabienataj D.A.A., Abuzadeh Mo., Omidi Mo., Numerical investigation on thermal performance of coiled tube with helical corrugated wall. International Journal of Thermal Sciences, 2021, 161: 106759.

[8] Zare M., Heyhat M.M., Performance evaluation of nanofluid flow in conical and helical coiled tubes. Journal of Thermal Analysis and Calorimetry, 2018, 135: 1–12.

[9] Jayakumar J.S., Mahajani S.M., Mandal J.C., Vijayan P.K. and Rohidas Bhoi, Experimental and CFD estimation of heat transfer in helically coiled heat exchangers. Chemical Engineering Research and Design, 2008, 86: 221–232.

[10] Pawar S.S., Sunnapwar V.K., Experimental and CFD investigation of convective heat transfer in helically coiled tube heat exchanger. Chemical Engineering Research and Design, 2014, 92: 2294–2312.

[11] Han Y., Wang X.S., Zhang H.N., Chen Q.Z., Zhang Z., Multi-objective optimization of helically coiled tube heat exchanger based on entropy generation theory. International Journal of Thermal Sciences, 2020, 147: 106150.

[12] Ahadi M., Abbassi A., Exergy analysis of laminar forced convection of nanofluids through a helical coiled tube with uniform wall heat flux. International Journal of Exergy, 2013, 13(1): 21–35.

[13] Kumar P., Kumar J., Suresh S., Babu K.P., Heat transfer enhancement in a helically coiled tube with Al_2O_3/water nano-fluid under laminar flow condition. International Journal of Nanoscience, 2012, 11(5): 1250029.

[14] Bahrehmand S., Abbassi A., Heat transfer and performance analysis of nanofluid flow in helically coiled tube heat exchangers. Chemical Engineering Research and Design, 2016, 109: 628–637.

[15] Narrein K., Mohammed H.A., Influence of nanofluids and rotation on helically coiled tube heat exchanger performance. Thermochimica Acta, 2013, 564: 13–23.

[16] Huminic G., Huminic A., Heat transfer and flow characteristics of conventional fluids and nanofluids in curved tubes: A review. Renewable and Sustainable Energy Reviews, 2016, 58: 1327–1347.

[17] Rainieri S., Bozzoli F., Cattani L., Pagliarini G., Experimental investigation on the convective heat transfer enhancement for highly viscous fluids in helical coiled corrugated tubes. Journal of Physics: Conference Series, 2012, 395: 012032.

[18] Zheng L., Xie Y.H., Zhang D., Numerical investigation on heat transfer and flow characteristics in helically coiled mini-tubes equipped with dimples. International Journal of Heat and Mass Transfer, 2018, 126: 544–570.

[19] Liu S., Masliyah J.H., Axially invariant laminar flow in helical pipes with a finite pitch. Journal of Fluid Mechanics, 1993, 251: 315–353.

[20] Chang L.M., Wang L.B., Song K.W., Sun D.L., Fan J.F, Numerical study of the relationship between heat transfer enhancement and absolute vorticity flux along main flow direction in a channel formed by a flat tube bank fin with vortex generators. International Journal of Heat and Mass Transfer, 2009, 52: 1794–1801.

[21] Lin Z.M., Sun D.L., Wang L.B., The relationship between absolute vorticity flux along the main flow and convection heat transfer in a tube inserting a twisted tape. Heat and Mass Transfer, 2009, 45(11): 1351–1363.

[22] Dang W., Wang L.B., Convective heat transfer enhancement mechanisms in circular tube inserted with a type of twined coil. International Journal of Heat and Mass Transfer, 2021, 169: 120960.

[23] Guo A.N., Wang L.B., The mechanism of laminar convective heat transfer enhancement enforced by twisting of elliptical tube. International Journal of Heat and Mass Transfer, 2020, 157: 119961.

[24] Song K.W., Shi W.N., Wu X., Wang L.B., Characteristics of flow symmetry and heat transfer of winglet pair in common flow down configuration. Symmetry, 2020, 12(2): 1–12.

[25] Song K.W., Wang L.B., The effectiveness of secondary flow produced by vortex generators mounted on both surfaces of the fin to enhance heat transfer in a flat tube bank fin heat exchanger. Journal of Heat Transfer, 2013, 135: 041902.

[26] Thompson J.F., Warsi S.W., Mastin C.W., Numerical grid generation-foundation and application. North-Holland, Amsterdam, 1985.

[27] Eriksson L.E., Practical three-dimensional mesh generation using transfinite interpolation. SIAM Journal on Scientific and Statistical Computing, 2006, 6(3): 712–741.

[28] Patankar S.V., Numerical heat transfer and fluid flow. Hemisphere, New York, 1980.